Ultrasonics 91 (2019) 180–192

Contents lists available at ScienceDirect

Ultrasonics

journal homepage: www.elsevier.com/locate/ultras

Optimization of USSP duration for enhanced corrosion resistance of AA7075

Vaibhav Pandey[a], J.K. Singh[b], K. Chattopadhyay[a,*], N.C. Santhi Srinivas[a], Vakil Singh[a]

[a] Department of Metallurgical Engineering, Indian Institute of Technology (Banaras Hindu University), Varanasi 221005, India
[b] Department of Architectural Engineering, Hanyang University, 1271 Sa 3-dong, Sangrok-gu, Ansan 426-791, Republic of Korea

ARTICLE INFO

Keywords:
Nanostructure
Ultrasonic shot peening
TEM
SEM
Polarization
EIS

ABSTRACT

This investigation was carried out following our earlier work on the effect of ultrasonic shot peening (USSP) on corrosion resistance of the 7075 aluminium alloy in 3.5 wt% NaCl solution to optimize the duration of USSP. The samples not treated with USSP and different samples treated with USSP were subjected to potentiodynamic polarization and electrochemical impedance spectroscopy. Among the specimens USSP treated from 5 to 30 s, the one USSP treated for 15 s (USSP 15) was found to exhibit highest corrosion potential (E_{corr}) and lowest corrosion current density (i_{corr}). Corrosion products were characterized by Scanning Electron Microscopy (SEM) and X-ray Photoelectron Spectroscopy (XPS). Scanning Kelvin Probe Force Microscopy (SKPFM) was used to measure the surface free potential. The enhanced corrosion resistance of the USSP 15 sample was found to be due to combined effect of surface nanostructure of the matrix, homogeneity and refinement of second phase precipitates. There was enhancement in formation of adherent passive layer in the USSP15 specimen.

1. Introduction

Peak aged aluminium alloys are widely used in aircraft, marine, automotive and construction industries because of their high specific strength, low cost and high corrosion resistance [1]. However, aluminium and its alloys are known to be susceptible to localized corrosion attack, especially in chloride environment [2]. Corrosion resistance of the 7075 aluminium alloy is also affected by the presence of different types of second phase particles like, $MgZn_2$, Mg_2Si, Al_7Cu_2Fe and Al_2CuMg [3–6], while some precipitates are anodic others are cathodic with respect to the aluminium matrix.

The performance of structural components subjected to fatigue, fretting fatigue, wear and corrosion strongly depends on their surface condition [7–9]. Ultrasonic shot peening (USSP) is a recently developed technique of grain refinement in surface region, even to nano scale, without altering the chemical composition of the material and has been applied successfully in various metallic materials such as steels [10,11] and alloys of Al [12,13], Mg [14] and Ti [15,16] for nanostructuring. This technique also induces compressive residual stress in the surface region along with grain refinement.

Al and its alloys possess good corrosion resistance because of dense and adherent layer of protective aluminium oxide on the surface. Some studies have been carried out on the effect of grain refinement at surface, on corrosion behavior of aluminium alloys, however, no attention has been paid on optimization of the process parameters for high corrosion resistance. It has already been well established by many investigators that fine-grained structure with more number of grain boundaries act as sites for passive layer formation and results in enhancement in corrosion resistance [17–19]. Chen et al. reported that surface nanocrystallization induced by shot peening resulted in enhancement in corrosion susceptibility of AA6061 [20]. Mordyuk et al. used ultrasonic peening on AISI 321SS for 1–4 min, and obtained optimal corrosion behavior with ultrasonic peening for 1 min and attributed it to increase of strain-induced martensite [10]. Song et al. [19] investigated corrosion behavior of ultrafine grained pure Al processed by ECAP and found improvement in pitting resistance. They attributed it to formation of stable passive layer of oxide from increased density of grain boundaries. Krawiec et al. [21] reported increase in charge transfer and in resistance of oxide film on AA2058-T8 due to presence of compressive residual stress resulting from laser shock peening treatment. High density of dislocations and grain boundaries provide active sites for easier formation of passive film whereas compressive residual stress makes the passive layer stable and integrated in respect of the untreated coarse grained counterpart [22]. Amit et al. [23] studied the role of multiaxial cryoforging (MAF) followed by ageing, on corrosion behavior of AA2024 and observed improvement in corrosion resistance. They attributed it to depletion of Cu and Mg from the matrix resulting from precipitation of the strengthening precipitates. Coarse second phase precipitates promote localized corrosion therefore absence or refinement of such precipitates leads to enhancement of the

* Corresponding author.
E-mail address: kausik.met@iitbhu.ac.in (K. Chattopadhyay).

https://doi.org/10.1016/j.ultras.2018.08.011
Received 15 February 2018; Received in revised form 3 July 2018; Accepted 16 August 2018
Available online 17 August 2018
0041-624X/

Table 1
Chemical composition of the alloy 7075 (wt%).

Zn	Mg	Cu	Si	Fe	Mn	Al
4.89	2.12	1.52	0.33	0.007	0.09	Bal.

corrosion resistance. The extent of deformation from USSP is a function of material as well as size of the ball, frequency of vibration and treatment time, therefore optimization of these parameters is mandatory in order to investigate the pronounced effect of this treatment on corrosion behavior.

The objective of the present investigation is to optimize the ultrasonic shot peening (USSP) duration for enhancement in corrosion resistance of this alloy. Corrosion properties are evaluated by potentiodynamic polarization and electrochemical impedance spectroscopy. X-ray photoelectron spectroscopy (XPS), Scanning kelvin probe force microscopy (SKPFM) and scanning electron microscopy (SEM) are used to characterize the observed corrosion behavior.

2. Experimental details

The AA7075 used in the present investigation was obtained from M/s Hindalco industries limited, Renukot, India. The chemical composition was determined using spark emission spectroscopy (FOUNDRY-MASTER) and is presented in Table 1. The material was studied in retrogression and re-aged (RRA) condition, solutionizing at 470 °C for 30 min, pre-ageing at 120 °C for 24 h, followed by retrogression at 200 °C for 10 min and subsequent secondary ageing at 120 °C for 24 h. USSP was performed for different durations of 5, 10, 15, 20, 25, 30 s and samples are designated as USSP 5, USSP 10, USSP 15, USSP 20, USSP 25 and USSP 30, respectively. The USSP operation was carried out using SONATS STRESSVOYAGER® with steel balls of 3 mm diameter at an amplitude of 80 μm.

The surface roughness of the USSP treated specimens was examined using Mitutoyo SJ-310 surface profilometer and the morphology was studied using JEOL 840A scanning electron microscope. Characterization of the phases and microstructure of the shot peened surface layer was carried out by XRD and TEM. X-ray diffraction was conducted using a PANalytical Empyrean X-ray diffractometer with CoK_{α} radiation. A TECNAI 20 G^2 transmission electron microscope, operating at 200 KV, was used to examine the nanograined surface microstructure of the USSP treated specimens. The plane view TEM foils were prepared from the top surface layer, mechanically polished from the un-treated side to thickness of about 50 μm, followed by electropolishing from the un-treated side using a twin jet electropolisher (TenuPol-5), at-30 °C at 20 V in a solution of 20% nitric acid in methanol. Scanning Kelvin probe force microscope (SKPFM) was used for surface potential of the without USSP and USSP treated specimens. An atomic force microscope (AFM) NTMDT, NTEGRA Prima with silicon probe was used in semi contact mode to determine the surface free potential.

Corrosion behavior of the without USSP and USSP treated samples was evaluated using potentiodynamic polarization (PD) and electrochemical impedance spectroscopy (EIS) in 3.5 wt% NaCl solution, at room temperature. A GAMRY™ Potentiostat (Series: PC-4) with three electrode cell consisting of saturated calomel electrode (SCE) as reference electrode, graphite as counter electrode and the specimen as working electrode was used. In order to stabilize the open circuit potential, the samples were exposed in 3.5 wt% NaCl solution prior to corrosion measurement. Potentiodynamic tests were carried out in potential range from -0.5 V to 1.5 V at a scan rate of 1 mV/s. EIS tests were performed imposing 10 mV sinusoidal voltage at open circuit potential of the test electrodes and changing the frequency between 100 kHz and 10 mHz. All the electrochemical studies were performed in triplicate to ensure reproducibility of the data. X-ray photoelectron spectroscopy (AMICUS, Kratos Analytical, Shimadzu) was used for chemical composition of the passive layer formed after 360 h of immersion. The Mg Kα line was used as X-ray source. The C 1 s peak was assumed to be at 285.4 eV and was used as an internal standard to determine binding energies of the other photoelectron peaks. XPS Spectra were mathematically fitted with Casa XPS software using a least square algorithm and a non-linear baseline.

3. Results

3.1. Microstructural analysis

3.1.1. Surface topography

Surface topography of the without USSP and different USSP treated samples was examined using SEM and optical profilometer and is shown in Fig. 1. It may be seen that surface of the without USSP sample is smooth whereas those of the USSP treated samples are rough. The depressions on surface of the USSP treated samples are due to impingement of the steel balls. Erosion was observed in surface region of the USSP 30 sample. The average surface roughness also increased with increase in the duration of USSP (Table 2) from continuous impingement of hard steel balls.

3.1.2. XRD analysis

Fig. 2 shows XRD patterns of the without USSP and the different USSP treated samples. There are peaks of only α-Al in all the specimens and there are no additional peaks from any other phase following the USSP. There is systematic shifting of diffraction peaks towards the lower angle side with increase in the duration of shot peening due to increase in the induced strain. The peak shift was 0.02, 0.02, 0.07, 0.03, 0.03 and 0.11 for the USSP5, USSP10, USSP15, USSP20, USSP25 and USSP30 respectively with respect to the without USSP specimen. There is broadening of peaks of the USSP treated samples due to grain refinement in the surface region. The average crystallite size was calculated using the Scherrer and Wilson equation [24].

$$t = \frac{0.9\lambda}{B\cos\theta_B} \tag{1}$$

Where t is the crystallite size, λ is X-ray wavelength, θ is Bragg angle and B is line broadening. The micro-strain was calculated using the Williamson Hall equation [25].

$$B\cos\theta = \left[\frac{0.9\lambda}{t}\right] + [4\varepsilon\sin\theta] \tag{2}$$

Where ε is root mean square of micro-strain. The calculated crystallite size and lattice strain from the XRD data are presented in Table 3. Grain size is found to decrease with increase in the duration of USSP and there is continuous increase in the microstrain. The crystallite size in all the USSP conditions is found to be in the range of nanometer.

3.1.3. TEM examination

The coarse-grained microstructure with some second phase precipitates in the aged condition of AA7075, is shown in Fig. 3(a). Inside the grains, metastable η' is semi-coherent with the matrix along with some pseudostable η, non-coherent with the matrix. Large particles of η are present in the grain boundaries. Microstructure of the top surface region is shown in Fig. 3(c) & (e) where ultrafine grained microstructure following USSP treatment for 15 and 30 s was observed. High strain rate during continuous peening of balls in surface region causes subdivision of the original coarse grains. The SAD pattern shows rings confirming formation of nanograins with high misorientations. With increase in the USSP duration from 15 to 30 s there was further refinement of grains which is evident from the SAD patterns with more continuous ring. Some precipitates are visible in the USSP 15 sample but not in the USSP 30, it may be due to dissolution/refinement of precipitates due to the USSP treatment.

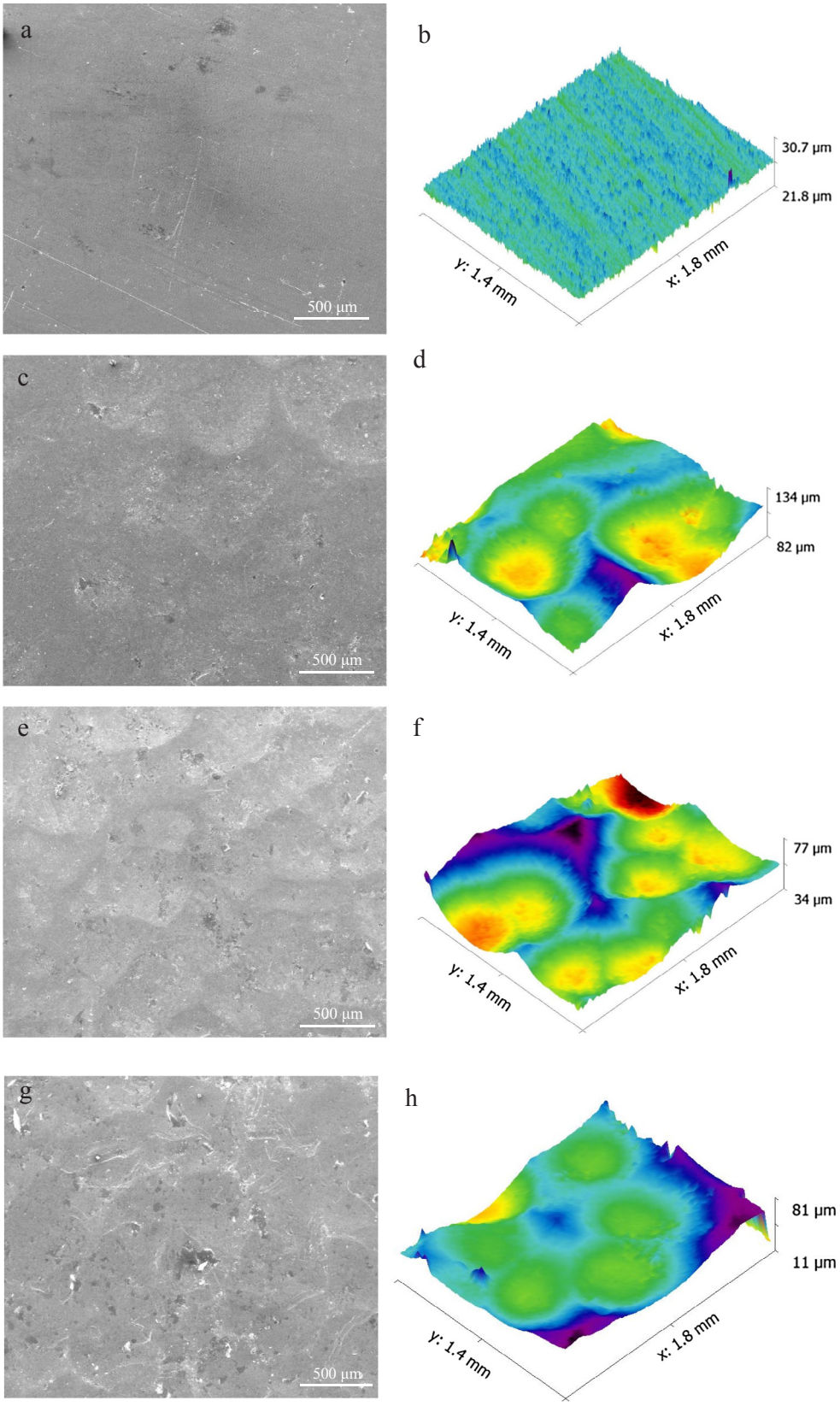

Fig. 1. Scanning electron micrographs and surface morphology of different specimens: (a, b) un-USSP; (c, d) USSP 5; (e, f) USSP 15 and (g, h) USSP 30 samples respectively.

Table 2
Average surface roughness of the without USSP and different USSP treated specimens.

Treatment condition	Average roughness (R_a)
without USSP	0.237
USSP 5	2.643
USSP 10	2.665
USSP 15	3.061
USSP 20	3.121
USSP 25	3.145
USSP 30	3.416

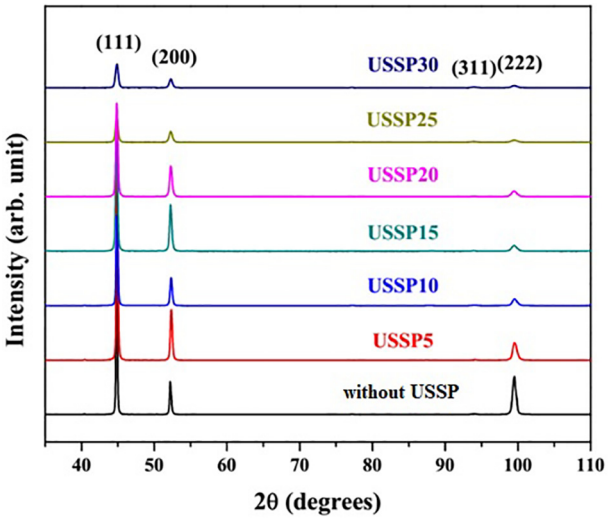

Fig. 2. X-ray diffraction spectrums of the without USSP and different USSP treated specimens.

Table 3
Average crystallite size and mean microstrain obtained from X-ray diffractogram.

Treatment condition	Crystallite size (nm)	Mean microstrain (%)
USSP 5	74.22	0.238
USSP 10	48.56	0.312
USSP 15	27.10	0.359
USSP 20	25.21	0.354
USSP 25	19.83	0.449
USSP 30	18.26	0.478

3.1.4. SKPFM study

Fig. 4 shows surface Volta potential of the without USSP and USSP 15 samples examined by in-situ AFM. There is difference in surface potential between the Al matrix and the surrounding intermetallic precipitates. From the line scan, it may be seen that Volta potential difference is positive at some places whereas it is negative at other places. In the without USSP condition, the brighter area represents intermetallics with higher potential. The intermetallic showing positive Volta difference (Fig. 4b) is cathodic in nature with respect to the matrix having +28 mV to +20 mV potential difference. Mainly these are Fe and Cu based second phase particles as reported earlier [26]. The anodic intermetallics are negative in nature with potential difference of −21 mV to −14 mV. This is due to the presence of Mg rich phases such as $MgZn_2$ and Mg_2Si [26]. For the USSP 15 sample the positive Volta potential difference lied in the range of +19 mV to +12 mV corresponding to Al matrix. Here the potential difference was less as compared to that of the without USSP sample, showing stronger galvanic coupling between the matrix and the intermetallics in the without USSP condition as compared to that in the USSP 15. On the other hand, there was very less effect on negative side of the Volta potential from −21 mV to −16 mV for the USSP 15 condition.

3.2. Corrosion behavior

3.2.1. Potentiodynamic polarization

Potentiodynamic polarization of the without USSP and the different USSP treated samples was carried out in 3.5 wt% NaCl solution following stabilization of the potential for 30 min. It is evident from the potentiodynamic plots in Fig. 5 that the samples USSP treated for more than 10 s show better corrosion resistance as compared with that of the without USSP as revealed by decrease in the anodic and cathodic current density. In the anodic region of the polarization curves there is continuous increase in the corrosion current density without any tendency of passivation for the without USSP, USSP 5 and USSP 10, whereas there are distinct passive regions for the USSP 15, USSP 20, USSP 25 and USSP 30 specimens, however, the degree of passivation is different for the different conditions. It is highest for the USSP 15, followed by USSP 30, USSP 25 and USSP 20 in decreasing order. The passive films break down at particular potentials characterized as pitting potential (E_{pit}), the values of E_{pit} are presented in Table 4. Pitting occurs due to localized damage of the oxide film by Cl^- ions. The resistance of the oxide films on the different samples may be seen from the difference between E_{pit} and E_{corr}, which is highest for the USSP 15. The increase in corrosion current of the USSP 15 to USSP 30 is due to breakdown of passive film which can be seen from Fig. 5.

The sudden increase in current density of the without USSP, USSP 5 and USSP 10 is due to breakage of the native thin layer of the passive oxide film during anodic scanning. On the other hand, the USSP 15 and the other specimens USSP treated for longer durations show passivation phenomena and the USSP 15 shows nobler passive region with lower current density. It may be seen from Fig. 5 that above E_{pit}, all the specimens exhibit limiting current density due to deposition of corrosion products which control the mass transfer at the interface of the specimen and solution. The limiting current density (i_{limit}) of the without USSP, USSP 5 and USSP 10 are around 26.75, 83.86 and 103.53 μA/cm^2 respectively at -0.750 V. However, as the USSP duration is increased, its value decreases and reaches lowest for the USSP 25. As the duration of USSP increased, the roughness also increased and accelerated the process of corrosion.

The electrochemical parameters such as corrosion current density (i_{corr}) and E_{corr} calculated by fitting the potentiodynamic curves in the Tafel region are shown in Table 4. The corrosion rate was calculated using the Platt equation.

$$Corrosion\ \ rate\ \ (\mu m/year) = \frac{3.27 \times 10^{-3} \times i_{corr} \times W_e}{d} \quad (3)$$

where the factor 3.27×10^{-3} includes the Faraday constant and the metric and time conversion factors, W_e represents the equivalent weight of Al alloy (9.98 g/mol), i_{corr} represents the measured corrosion current density (μA/cm^2), and d represents the density of the corroding element (2.81 g/cm^3). Corrosion rate for the without USSP sample as recorded in Table 4 is found to be 44.19 μm/year whereas it is reduced to 20.06 μm/year for the USSP 15. The corrosion rate increases abruptly for the specimens treated initially up to 10 s, however, as the treatment time is increased up to 15 s its value is considerably reduced. Beyond this period of the USSP treatment, again corrosion rate is increased again.

For the USSP 15 specimen, the value of E_{corr} shifted towards the nobler potential compared to that of the without USSP and those of the other USSP treated samples. The other USSP treated treated specimens exhibited E_{corr} in between −0.770 and −0.785 V whereas the without USSP exhibited -0.839 V which is more active than USSP treated 15 (−0.695 V). This result suggests that the USSP treated 15 specimen forms protective and passive film on the surface in 3.5 wt% NaCl solution. The E_{pit} and E_{corr} for the USSP 5 and USSP 10 are almost

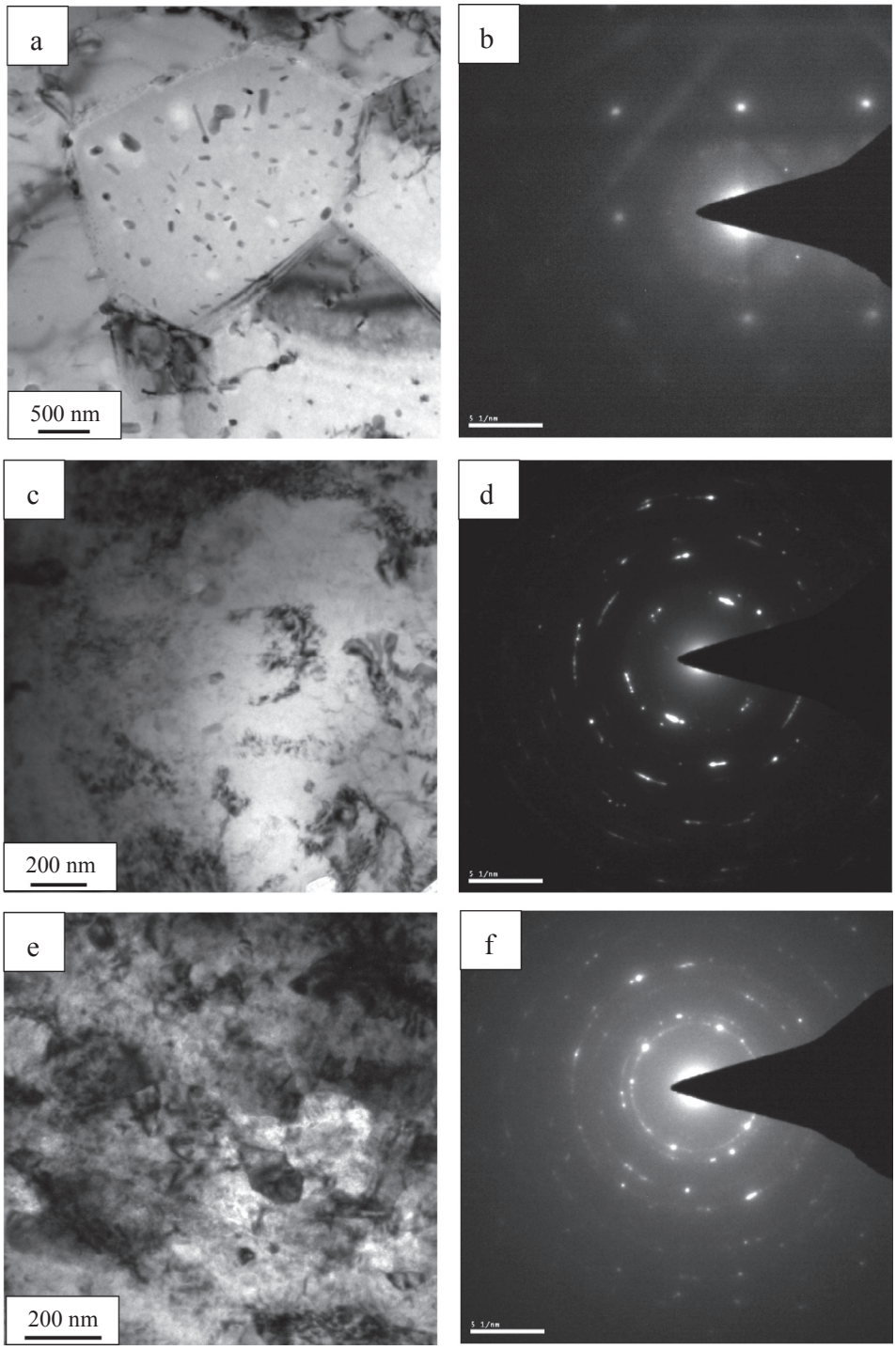

Fig. 3. Transmission electron micrograph and its corresponding SAED pattern of different specimens: (a, b) without USSP, (c, d) USSP 15 and (e, f) USSP 30 condition respectively.

identical which reveals that these specimens are more active for pit formation due to USSP treatment. The most positive value of corrosion potential and lowest values of i_{corr} is shown by the USSP 15 sample showing lower dissolution rate and best corrosion resistance amongst all the tested specimens.

3.2.2. Electrochemical impedance

In order to have the interfacial information at the metal/solution interface in the aggressive environment, EIS was carried out in 3.5 wt% NaCl solution for different durations of exposure. Prior to EIS, samples were kept in 3.5 wt% NaCl solution for stabilization of the potential. The Nyquist plots for the durations of exposure of 24 h and 360 h are shown in Fig. 6a and d respectively. It may be seen that Nyquist plots for all the specimens are similar in shape but differ in diameter for the different durations of exposure. As the exposure period was increased up to 360 h (Fig. 6d), the diameter of the Nyquist plots at lower and higher frequencies was reduced. This suggests that all the specimens exhibited deterioration in corrosion properties for longer duration of exposure. However, the USSP 15 shows larger diameter of the Nyquist plots at lower frequency where the tail is longer compared to those of the other specimens. In the range of higher to middle frequency, the diameter of Nyquist plots even for 360 h of exposure is larger in size

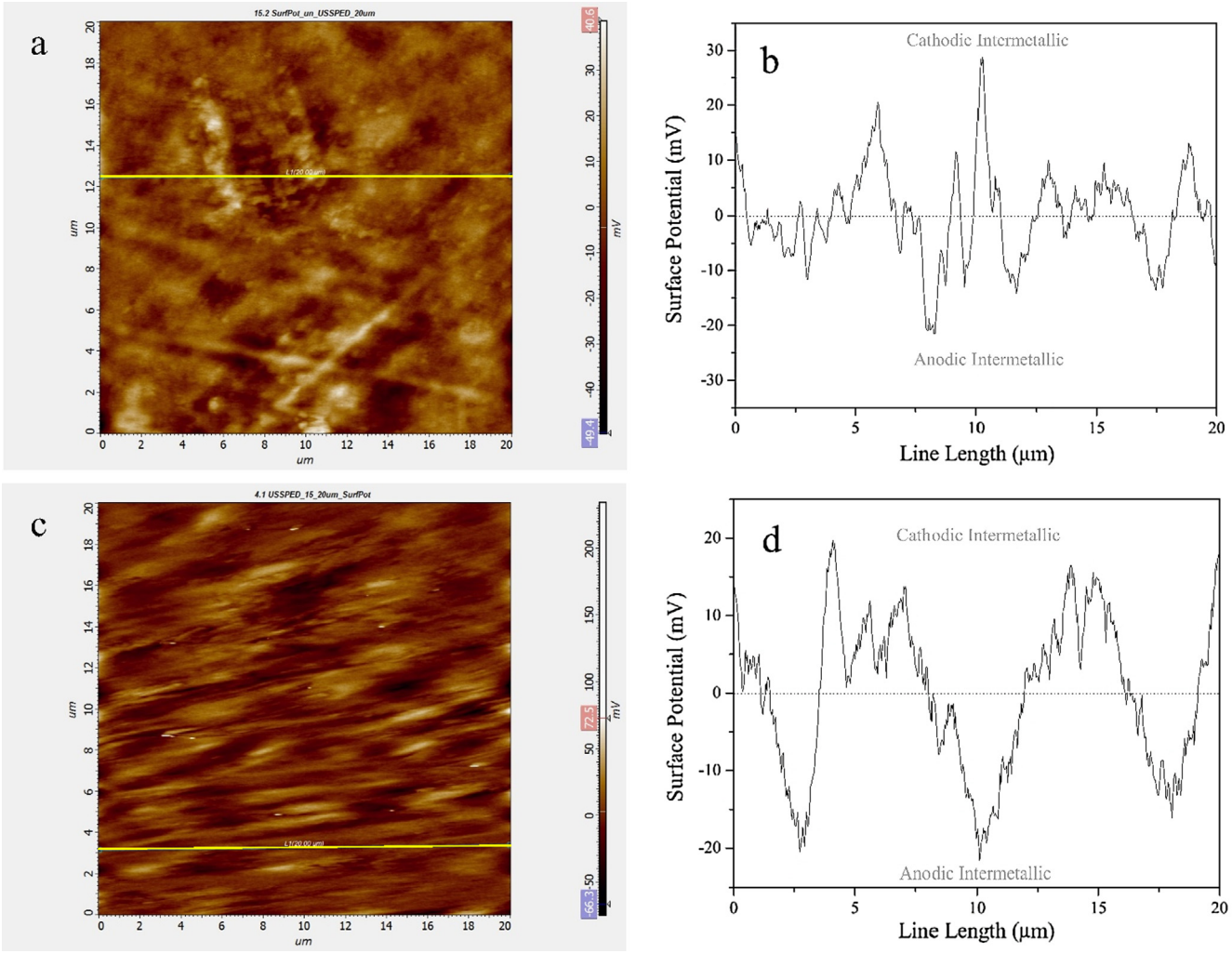

Fig. 4. Volta potential map (a, c) and linear distribution of potential (b, d) for without USSP and USSP 15 samples respectively.

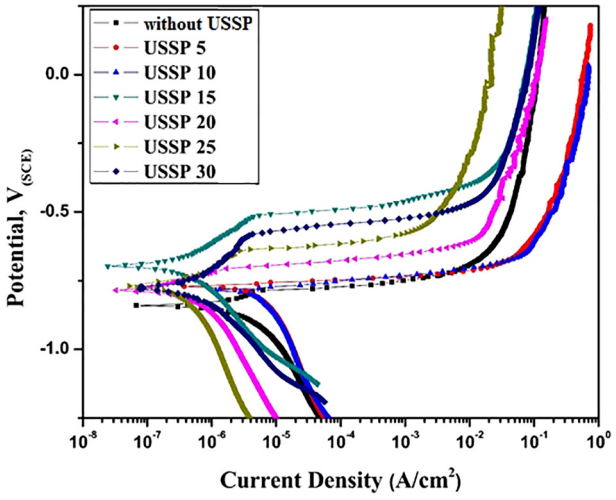

Fig. 5. Potentiodynamic polarization curves in 3.5 wt% NaCl solution, after 30 min of their exposure.

than those of the other specimens.

The log modulus-frequency Bode plots for the tested specimens are shown in Fig. 6b and e. It can be seen from Fig. 6b that after 24 h of exposure in 3.5 wt% NaCl solution, the USSP 15 specimen shows highest impedance compared with the others at the lowest studied frequency of 0.01 Hz. The impedance decreased for the USSP 10 sample and is less for the without USSP specimen. The impedance is maximum for the USSP 15 sample, however, beyond this it tends to decrease. As the period of exposure increased up to 360 h in 3.5 wt% NaCl, the impedance gradually decreased for all the specimens (Fig. 6e). The trend is identical to that after 24 h of exposure, for all the specimens.

The phase-frequency Bode plots of the specimens exposed in 3.5 wt % NaCl solution are shown in Fig. 6c & f. From this it can be seen that the USSP 15 specimen exhibits two inflections (two-time constants) at different frequencies, one in the range of middle frequency which indicates capacitive properties of the passive film that formed during the process of corrosion while the other one in the range of lower frequency

Table 4
Electrochemical parameter of the without USSP and USSP treated 7075 aluminium alloy in 3.5 wt% NaCl solution, after 30 min of their exposure.

Treatment condition	E_{corr} (V)	i_{corr} (μA/cm^2)	E_{pit} (V)	$E_{corr} - E_{pit}$ (V)	Corrosion rate (μm/year)
without USSP	−0.839	1.269	−0.790	−0.049	44.19
USSPed 5	−0.770	2.99	−0.759	−0.011	102.61
USSPed 10	−0.785	5.13	−0.778	−0.007	176.02
USSPed 15	−0.695	0.564	−0.517	−0.178	20.06
USSPed 20	−0.786	0.68	−0.707	−0.079	26.67
USSPed 25	−0.772	0.78	−0.642	−0.130	30.73
USSPed 30	−0.778	1.07	−0.596	−0.182	38.10

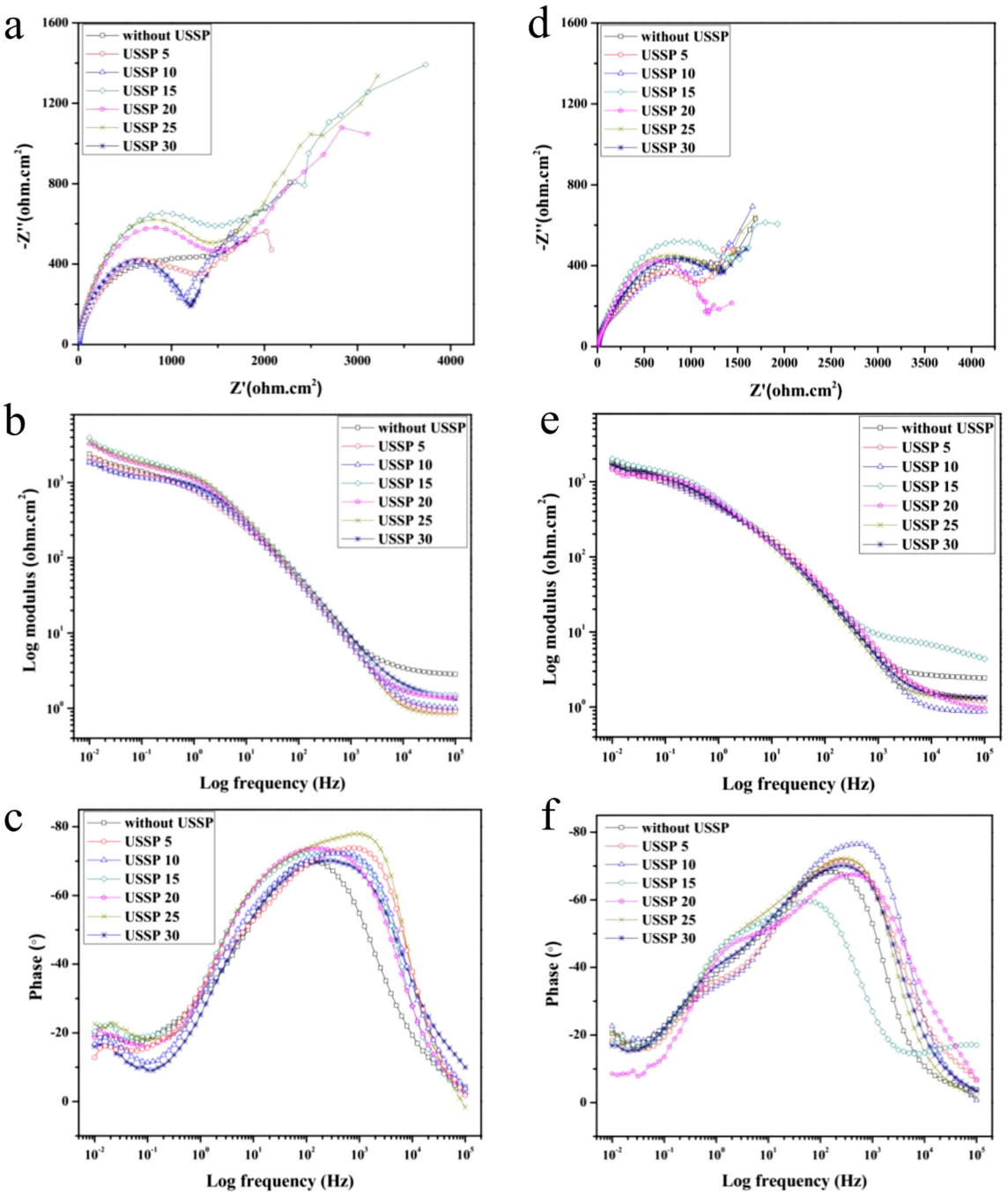

Fig. 6. EIS plots of the without USSP and different USSP treated samples in 3.5 wt% NaCl solution recorded at their respective open circuit potentials for immersion duration of (a-c) 24 h and (d-f) 360 h respectively.

indicating occurrence of reaction at metal/solution interface. All the USSP treated specimens except the USSP 15 and the un-treated specimen exhibited only one-time constant at middle frequency range. It can be seen from Fig. 6c that at lower frequency, the phase angle maxima of the USSP 15 specimen for the first-time constant shifted towards −22° while its second-time constant gradually shifted at middle frequency around −70°. On the other hand, the other specimens show shifting of maxima at higher frequency compared with USSP 15. The USSP 15 covers the broaden range of studied frequency around −70° which suggests formation of capacitive passive film reducing the active surface area of the Al alloy for corrosion [27,28]. As the exposure period is increased from 24 h to 360 h (Fig. 6 f), the decrease in phase angle maxima is due to the deterioration in properties of the without USSP and USSP treated specimens in 3.5 wt% NaCl solution. Even though after 360 h of exposure, USSP 15 specimen exhibited two-time constants and in this case, the first-time constant shifted from lower to middle frequency i.e. 100 Hz around -50°. From this figure, it can also be seen that the other USSP treated specimens and the without USSP specimen exhibited shifting of maxima towards higher frequencies revealing that corrosion would have induced in the specimen at longer duration of exposure. Thus, it may be seen that the optimum treatment time for the highest corrosion resistance of the AA7075 is 15 s and below or above this duration, the alloy is susceptible to higher rate of corrosion in 3.5 wt% NaCl solution [28].

EIS spectra of the without USSP and different USSP treated specimens are fitted with suitable electrical circuit shown in Fig. 7 and the

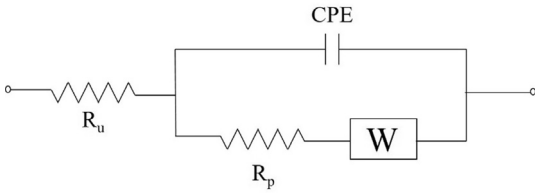

Fig. 7. Equivalent electrical circuit.

values of different EIS parameters are shown in Table 5. Such type of circuit has already been established by Domínguez-Crespo et al. for Al metal surface exposed in 3.5% NaCl solution [29]. In this model R_p is polarization resistance, R_u is solution resistance between solution and the reference electrode, Q is constant phase element (CPE) parameter, W_d is Warburg diffusion coefficient and alpha (α) is CPE exponent.

3.2.3. Potentiodynamic study after 360 h of exposure

Corrosion characteristics of the oxide/passive film formed on surface of the without USSP and USSP treated samples was examined by potentiodynamic studies after 360 h of exposure in 3.5 wt% NaCl solution. The potentiodynamic plots are shown in Fig. 8 and the different calculated corrosion parameters are presented in Table 6. The anodic reaction for all the conditions started from their respective E_{corr} and passive regions formed at 1.5–2.0 μA/cm^2 up to −0.730 V. The transpassive region is observed around −0.750 V up to −0.300 V at 0.64 μA/cm^2 to 7.11 μA/cm^2 anodic current density except for the without USSP and USSP 5 specimens which was found to be up to −0.467 V, thereafter E_{pit} started. The without USSP specimen exhibited i_{lim} at 189.0 μA/cm^2 at −0.361 V due to deposition/formation of large amount of porous corrosion products. After careful analysis of the extracted electrochemical data in Table 6 it can be inferred that the E_{pit} of the USSP 15 is noble (−0.281 V) and I_{corr} is 2–7 times lower than those of the other specimens. It reflects the excellent adherent and protective nature of the passive film formed on its surface. On comparison of potentiodynamic results after 30 min and 360 h of exposure, it is found that at longer duration of exposure all the specimens show higher corrosion, but among them the USSP 15 is the best from the point of view of corrosion resistance in 3.5 wt% NaCl solution.

3.2.4. X-ray photoelectron spectroscopy

XPS characterization was carried out for the specimens before (unexposed) and after 360 h of EIS in 3.5 wt% NaCl. High resolution XPS curve fitted spectra are presented in Fig. 9. In the fitted spectra of the without USSP and USSP 15 specimens before exposure to 3.5 wt% NaCl are shown in Fig. 9a and c, respectively and two peaks appeared. The first peak of higher intensity from Al_2O_3 may be seen to appear at

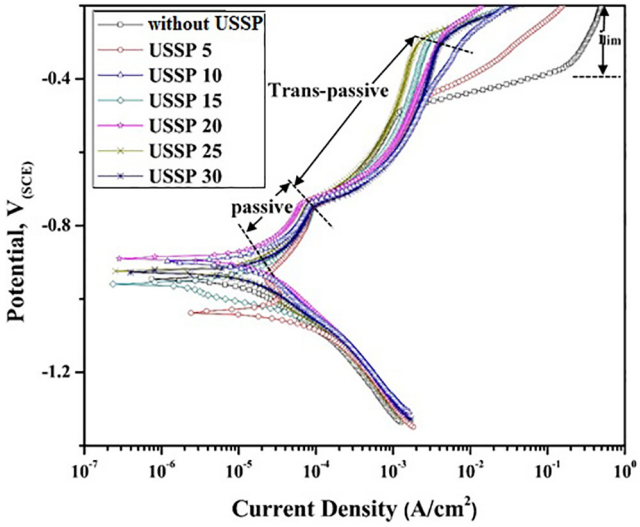

Fig. 8. Potentiodynamic polarization curves of the without USSP and USSP treated specimens after 360 h of exposure in 3.5 wt% NaCl solution.

Table 6
Electrochemical parameter of the without USSP and USSP treated specimens after 360 h of exposure in 3.5 wt% NaCl solution.

Treatment condition	E_{corr} (V)	i_{corr} (μA/cm^2)	E_{pit} (V)	Corrosion rate (μm/year)
without USSP	−0.947	27.20	−0.467	917.44
USSPed 5	−1.030	31.60	−0.467	1065.78
USSPed 10	−0.900	40.70	−0.294	1373.37
USSPed 15	−0.959	6.260	−0.281	211.09
USSPed 20	−0.889	12.10	−0.298	407.41
USSPed 25	−0.924	17.60	−0.298	592.58
USSPed 30	−0.928	18.10	−0.298	612.14

74.7 eV and 74.6 eV whereas the second peak from the matrix appeared at 71.9 eV and 71.6 eV for the without USSP and USSP 15 specimens respectively. After the exposure of 360 h in the 3.5 wt% NaCl an additional peak of $Al(OH)_3$ along with the peaks of Al_2O_3 and Al matrix was also observed in the without USSP condition. On the other hand, for the USSP 15 condition only two peaks, one of Al_2O_3 and the other of $Al(OH)_3$ were observed and peak of Al matrix was absent. The appearance of $Al(OH)_3$ peak after exposure suggests change in chemical state of the surface.

Table 5
EIS parameters of the without USSP and USSP treated samples for different exposure durations in 3.5 wt% NaCl solution recorded at their respective open circuit potentials.

Treatment Condition	Immersion time (h)	Electrochemical parameters					
		R_u (Ω cm^2)	R_p (Ω cm^2)	Y_0 (Ω^{-1} cm^{-2}Sn) (×10^{-5})	α	W_d (Ss$^{1/2}$ × 10^{-3})	Chi-Square (×10^{-3})
without USSP	24	2.828	994.5	10.91	0.80	2.645	5.171
	360	2.275	723.4	17.4	0.78	3.021	16.31
USSP 5	24	0.774	959.1	11.3	0.80	3.097	17.55
	360	0.750	646.6	19.4	0.77	3.571	18.11
USSP 10	24	0.928	946.4	11.6	0.80	4.259	5.013
	360	0.806	402.0	39.4	0.60	5.540	23.46
USSP 15	24	1.368	1470	7.79	0.85	1.70	4.840
	360	5.209	1403	8.59	0.84	1.737	13.46
USSP 20	24	1.328	1349	8.66	0.82	1.953	2.567
	360	0.842	1163	9.72	0.81	2.037	11.25
USSP 25	24	0.764	1297	8.99	0.81	2.151	10.52
	360	1.174	962.0	11.5	0.79	2.691	16.67
USSP 30	24	1.297	1091	9.71	0.81	2.20	1.906
	360	1.195	855.0	16.1	0.78	2.830	17.29

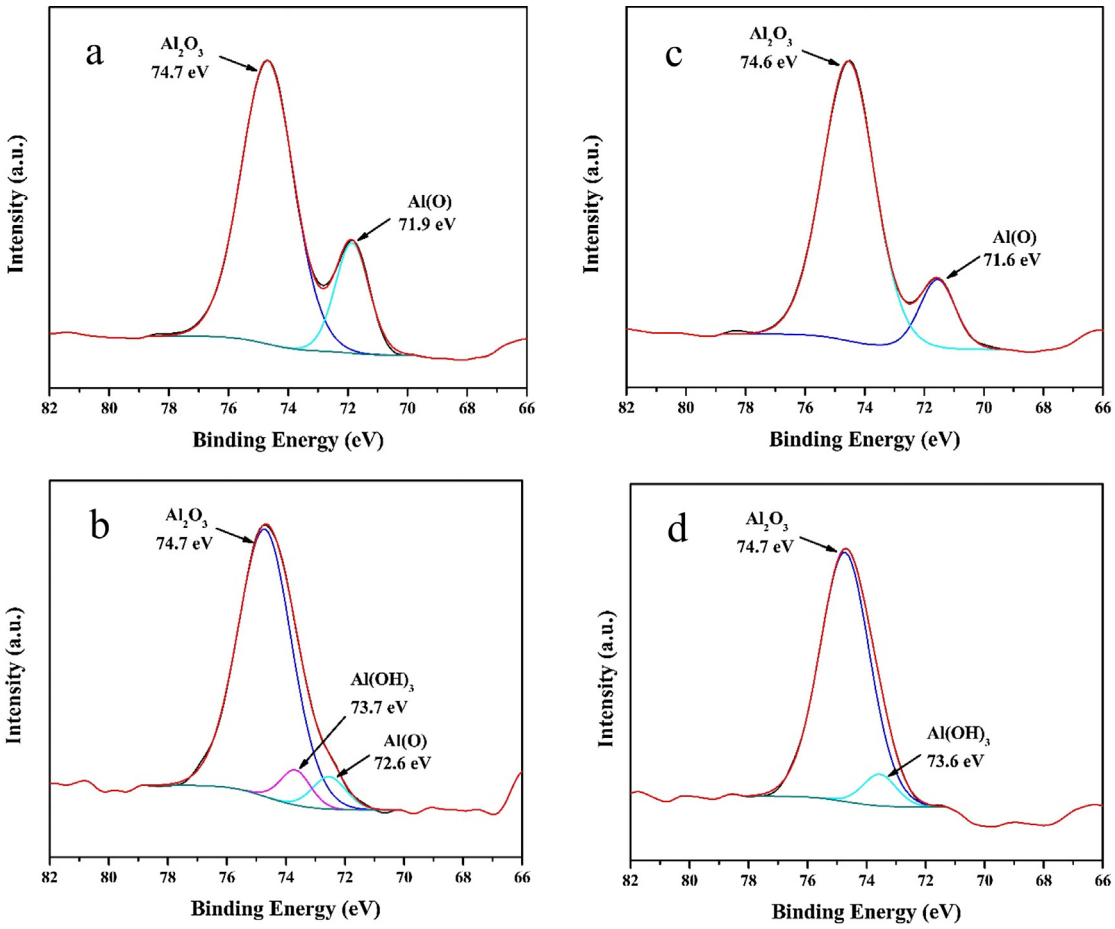

Fig. 9. XPS Al2p spectrum of different samples: (a) without USSP, (b) without USSP + 360 h of exposure, (c) USSP 15 and (d) USSP 15 + 360 h of exposure.

4. Discussion

Potentiodynamic polarization curves clearly show enhanced corrosion resistance of the samples USSP treated for 15–30 s. I_{corr} and E_{corr} values are the measure of corrosion resistance. The USSP 15 sample showed lowest I_{corr} and nobler E_{corr} which clearly indicate higher corrosion resistance. The USSP 20, USSP 25 and USSP 30 samples also showed better corrosive properties than that of the without USSP. Anodic portion of polarization curves of the samples show continuous increase in current density with some tendency of passivation for the USSP 15, USSP 20, USSP 25 and USSP 30 samples. The range of passive plateau is highest for the USSP 15 followed by the USSP 30, USSP 25 and USSP 20. This suggests that an anodic potential shift of passive plateau of about -0.178 V is due to the stability of the passive film which is attributed to presence of nanocrystalline surface layer [30]. Increase in current density is due to initiation of localized corrosion. The rapid increase in current density after passivation is designated as pitting potential (E_{pit}). The USSP 15 sample shows passivation up to −0.517 V from its OCP (open circuit potential) before the breakdown, whereas passive region was not present in the case of USSP 5 and USSP 10 samples. It was due to rapid increase in the roughness from USSP treatment which hindered the formation of passive layer.

The SEM micrographs of the without USSP and USSP 15 sample after potentiodynamic polarization (Fig. 10) shows that there was pitting tendency over entire surface of the specimen. Severe pitting was observed on surface of the without USSP sample as compared with that of the USSP 15. It is clear from EDS analysis of the pits (indicated by circle) that pits are enriched by Mg, Zn and Si suggesting that pitting has occurred mainly close to the second phase particles or the precipitates and the bright and large size particles are mainly the corrosion product of Al_2O_3. In the without USSP condition it is due to the coarse intermetallic particles, mainly along the grain boundaries which cause localized corrosion and breakdown immediately above the E_{corr}. Therefore, the presence of intermetallic particles like Mg_2Si and coarse $MgZn_2$ precipitates at the grain boundaries leads to higher corrosion rate in the without USSP condition [31]. For the USSP 15 sample the severity of pitting was rather less and was confined to isolated regions which could be defects, craters or second phase particles. These particles act either anodic or cathodic with respect to matrix and cause localized corrosion [32]. This is due to galvanic coupling between the precipitates and the matrix because of the potential difference between them. In the USSP 15 condition the second phase particles could have undergone dissolution therefore there were very less active sites on the surface for corrosion to occur. It was also confirmed by the SKPFM studies (Fig. 4) that the volta potential difference was less for the USSP 15 as compared to that of the without USSP, indicating a stronger galvanic coupling for the without USSP condition. Therefore, USSP 15 sample exhibited better corrosion resistance than that of the without USSP [33].The anodic intermetallics have the same volta potential (-21 mV) in both without USSP and USSP 15 condition, whereas there is some difference in volta potential for the cathodic intermetallics (+28 mV & +19 mV). Hence, the corrosion resistance of the 7075 aluminium alloy can be attributed to difference in volta potential of the cathodic intermetallics.

It can be explained from the schematic in Fig. 11 that in case of the without USSP samples the coarse second phase particles cause localized corrosion and lead to large size pits, whereas in the USSP treated samples the refinement/dissolution of the second phase particles restricts the tendency of localized corrosion. The area surrounding the particles shows galvanic coupling which is more in the without USSP

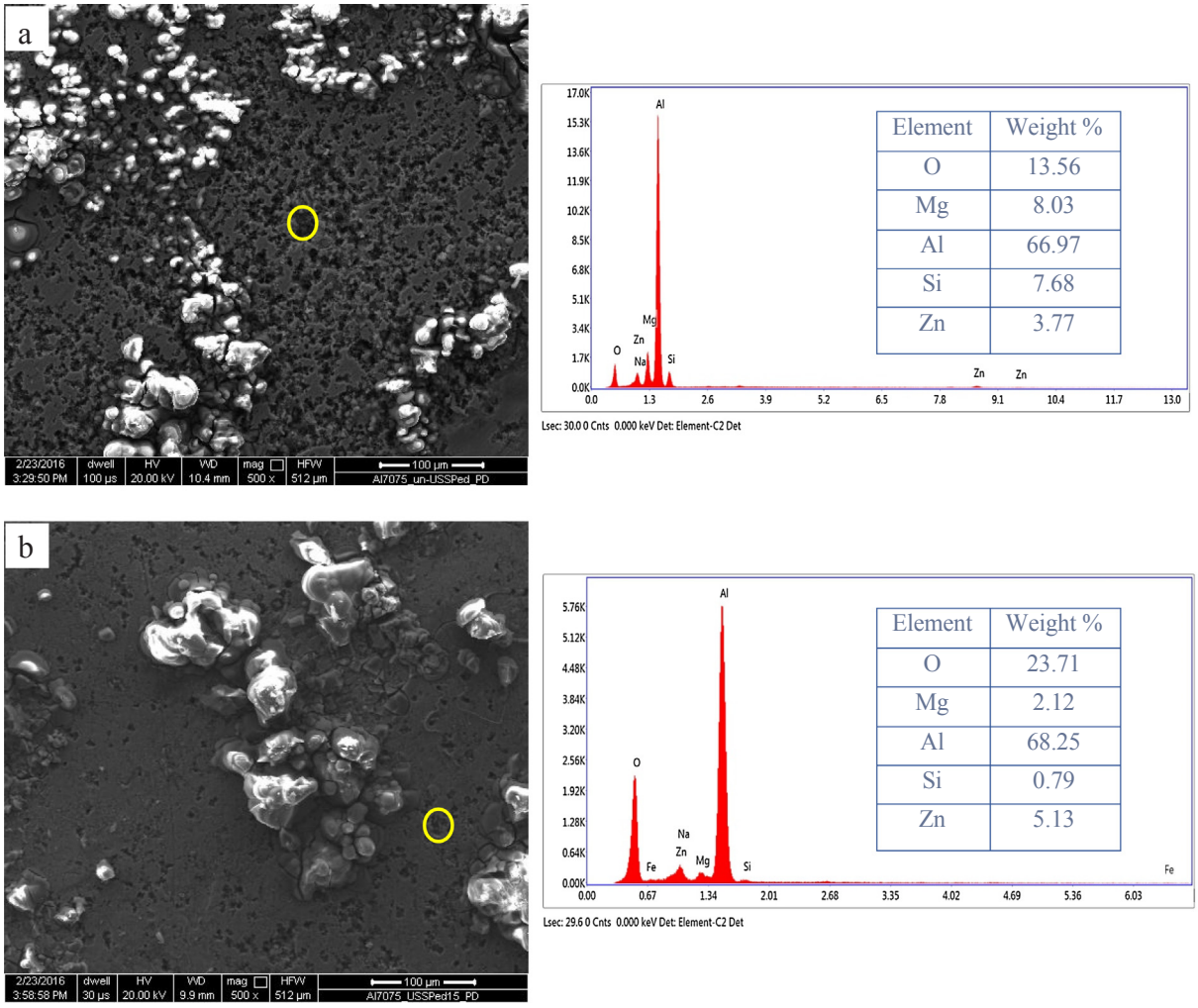

Fig. 10. Morphology and its corresponding EDS results of AA7075 after potentiodynamic polarization in 3.5 wt% NaCl solution (a) without USSP and (b) USSP 15.

condition due to large volta potential difference whereas it is found to be less in the USSP 15 condition. Due to this there was formation of a very thin and stable passive layer on the surface of the USSP 15 sample. Hence, the enhanced corrosion resistance of the USSP 15 sample may be attributed to nanostructured surface layer and finer second phase precipitates.

In the Nyquist plot, there was formation of two depressed semi-circle loops for the both 24 h as well as 360 h of exposures. It can be seen from Fig. 6a and d that the samples not treated with USSP and all the USSP treated samples exhibited a depressed semi-circular loop in the complex impedance plane with the center under the real axis (Z'_{real}), which is a typical behavior of solid metal electrodes showing frequency dispersion in the impedance data [34,35]. Also, all the specimens show a tail in the region of lower frequency which can be attributed to thin oxide film or diffusion control process [36,37]. The semi-circular loop at higher frequency is due to the resistance caused by

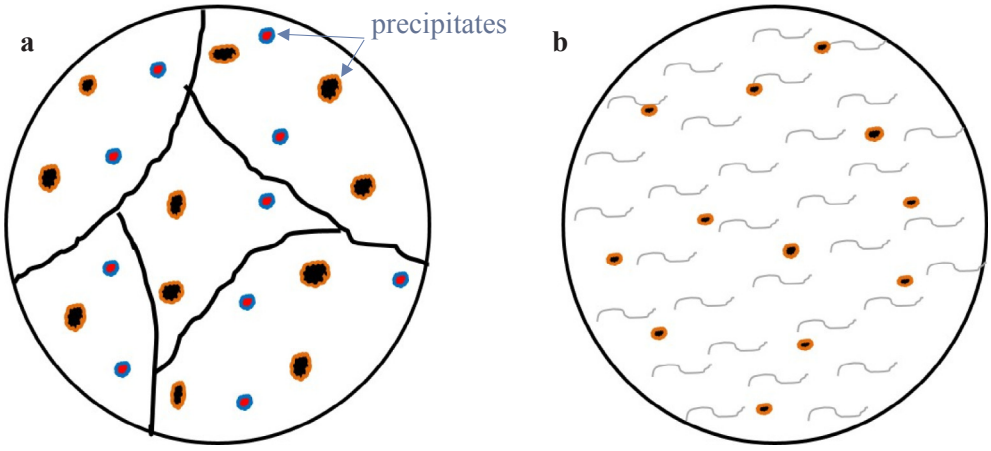

Fig. 11. Schematic showing surface morphology of (a) without USSP and (b) USSPed specimen.

oxide film formed on metal/solution interface and capacitance of the charge transfer process while at lower frequency a straight line reveals the Warburg impedance which shows characteristic features of diffusion within the Al alloy specimen [38,39]. The $MgZn_2$ precipitates on the surface of the alloy 7075 are susceptible to Cl^- ions and undergo dissolution in the without USSP condition whereas these precipitates get fragmented in the samples USSP treated for higher durations. Initially, for the USSP treated samples the formation of passive film is enhanced when it reacts with NaCl. On much longer exposure of 360 h, the diameter of the loop is decreased due to formation of thick and defective oxide layer which caused decrement in the polarization resistance (R_p). These results clearly show that the passive film formed on the USSP treated samples is not effective for longer duration of exposure, however, it is much better as compared to that formed on the without USSP specimen.

The log modulus-frequency plots show that the impedance was highest for the USSP 15 sample at the frequency of 0.01 Hz for the both, 24 h as well as 360 h of exposures in 3.5 wt% NaCl solution and thus further strengthens the observed high corrosion resistance of USSP 15. The highest impedance of the USSP 15 sample is attributed to formation of highly effective passive film on the surface, being more resistant to penetration of Cl^- ions, than the films formed on the other USSP treated samples. However, its resistance is reduced on long exposure of 360 h (Fig. 6e). With further increase in the USSP duration the impedance was found to decrease, suggesting that as the USSP duration is increased the surface becomes more susceptible to Cl^- ions attack. It was lowest for the USSP 10 sample, which may be attributed to abrupt increase in surface roughness interfering the formation of protective passive layer to reduce the corrosion resistance. On longer duration of exposure of 360 h the impedance was found to decrease for all the conditions, suggesting that oxide layer is porous in nature and the initially formed passive layer is thin which becomes less stable and prone to ingress of Cl^- ions, hence impedance is decreased. In phase-frequency plots broad phase angle peak is observed for 24 h of immersion, whereas the maxima is narrower and gets shifted towards lower phase after 360 h of exposure (Fig. 6f). The shifting of maxima towards lower phase indicates deposition of corrosion products on the surface. In the electrochemical equivalent circuit, W_d is due to the diffusion process taking place, indicating porous and inhomogeneous nature of the passive/oxide film. The diffusion coefficient was found to increase on 360 h of exposure for each tested condition. It reflects less effectiveness of the oxide film formed in checking the flow of aggressive ions towards the substrate [40].

Three regions were distinguished from the polarization curve after 360 h of exposure (Fig. 8) in 3.5 wt% NaCl solution. The Al^{3+} ions are generated after oxidation of Al whereas OH^- ions are released after oxygen reduction reaction (equation (2). The passive region might form from the transformation of $Al(OH)_3$ into Aluminum oxide on the surface during prolong exposure [41].

$$H_2O + \tfrac{1}{2}O_2 + 2e^- \rightarrow 2OH^- \quad (4)$$

$$Al^{+++} + 3OH^- \rightarrow Al(OH)_3 \quad (5)$$

$$2Al(OH)_3 \rightarrow Al_2O_3 \cdot 3H_2O \quad (6)$$

$Al(OH)_3$ is insoluble in neutral pH solution and gets accumulated at the interface of metal/solution of the Al alloy and results in formation of corrosion products [42]. During anodic scanning, $Al(OH)_3$ oxidizes into aluminum oxide with increase in potential in another region and subsequently gets accumulated on the alloy which is main reason for the formation of passive region. The different corrosion characteristics of the Al alloy shown after 360 h of exposure in 3.5 wt% NaCl solution is due to heterogeneous microstructure, impurities, segregation, morphology, distribution of second phase precipitates attributed to surface treatment [43].

In 3.5 wt% NaCl neutral pH solution, the anodic current in passive region is almost consistent, low and identical, due to suppressed uniform corrosion by neutral oxide layer (Al_2O_3). The cathodic current density is dependent on size and volume fraction of precipitates which act as local cathode and the volume of oxidant such as dissolved oxygen dominates over the reaction. The solution containing Cl^- ions accelerates the corrosion process of Al alloy by attacking on oxide films. Thus, gradual increment in anodic current is observed after passive region due to attack of Cl^- ions on applied potential which causes dissolution of the aluminum oxide (Eq. (5)). This corrosion product (Al_2O_3) has dual nature, the inner layer is adherent, compact and stable whereas the outer layer is porous, less stable and more susceptible to corrosion [44,45]. This high concentration of Cl^- ions led to breakdown of the oxide film and formed trans-passive region according to following reactions [46,47]:

$$Al \rightarrow Al^{3+} + 3e^- \quad (7)$$

$$Al^{3+} + 4Cl^- \rightarrow AlCl_4^- \quad (8)$$

After the trans-passive region, the polarization curve shows limiting current which was due to the deposition of thick corrosion product.

XPS results suggest that a layer of Al_2O_3 is present for the both without USSP as well as USSP 15 samples as shown by the peak at 74.7 eV (Fig. 9a & c). The first peak at 74.7 eV of Al_2O_3 has intensity higher than the second at 71.9 eV of Al matrix, this indicates that the oxide layer is thin. The self-passivation for the USSP 15 was highest as the intensity of matrix peak for the USSP 15 was relatively lower as compared to that of the without USSP [7]. The increased area of grain boundaries promotes passivation tendency of the oxide layer [48]. There is formation of thicker oxide layer over the surface of the USSP treated specimens due to the presence of nanocrystalline surface layer. After 360 h of exposure for the USSP 15 specimens no peaks of Al matrix were observed whereas as it was there for the without USSP, which clearly indicates that the layer formed on the surface of the specimen was more homogeneous. Trdan et. al [28] showed that laser shock peening process transforms the amorphous Al_2O_3 into more stable oxide which resulted in improved corrosion resistance. From the XPS results it can be derived that the protective layer of Al_2O_3 along with $Al(OH)_3$ resulted in enhanced corrosion resistance of the USSP treated specimens.

USSP treatment effectively induces nanocrystalline layer on the surface of the 7075 aluminium alloy. Corrosion current density and corrosion potential of the USSP 15 suggest enhanced corrosion resistance. Severe plastic deformation caused grain refinement and thus increased grain boundaries and dislocation density. The fine-grained layer with more number of grain boundaries reduces the chloride concentration per grain boundary thus resulting in lesser current density [49,50]. Polycrystalline materials are attacked preferentially during corrosion due to segregation of impurities, imperfect atomic structure and high energy [51]. High density of grain boundaries and dislocations act as sites for passive layer formation and suppress dissolution in the passive state [17,18,52]. The higher charge transfer resistance of the passive film in the EIS result indicates higher stability of the passive film even after prolonged duration of exposure. The refinement/dissolution of the second phase precipitates was also observed after the USSP treatment. Homogeneous distribution of refined precipitates throughout the matrix promotes formation of adherent and uniform passive layer. It has been reported that passive film may be different in stability or may even be absent on second phase in aluminium alloys [53]. For ultrafine grained Fe-Cr alloy higher concentration of Cr was reported at the surface than in the coarse-grained counterpart and this enrichment of Cr at the surface resulted in higher passivation [54]. Therefore, for USSP treated sample a more stable and uniform passive film was formed on the surface causing more positive corrosion potential and smaller current density.

Plastic deformation imparts residual stress near the surface region which is mostly compressive in nature. The extent and intensity of

compressive residual stress depends on the USSP treatment parameters. Takakuwa et al. [55] reported reduction of inter atomic spacing enables growth of passive layer due to compressive stress. The corrosion current density decreased with increase in compressive stress and this improves corrosion resistance. In the present study also the induced compressive stress resulting from USSP treatment would have facilitated the formation of passive layer over the surface of the USSP 15 specimen. Krawiec et al. [21] found increment in charge transfer and oxide film resistance after ageing in air, due to the compressive residual stresses resulting from laser shock peening (LSP) treatment which resulted in enhancement in electrochemical behavior of AA2050-T8. Trdan et al. [56] studied the effect of LSP on corrosion behaviour of AA6082-T65 in 3.5% NaCl solution and found that LSP improves corrosion resistance, reduces surface pitting and intergranular attacks. This could be attributed to the low surface roughness in LSP in comparison to SP, as well as higher induced compressive residual stresses.

The plastic deformation resulting from USSP treatment induced high density of dislocations near the surface region of the alloy. It has been reported that increase in dislocation density provides active sites for corrosion [57]. With increase in USSP duration the extent of deformation increases which also results in increment in dislocation density. Increase in the size of balls and treatment duration of SMAT increases the extent of deformation which reduced the corrosion rate of 409SS [58]. Increase in corrosion rate for the samples treated beyond the duration of 15 s may be attributed to increase in dislocation density and the surface defects. Although for some cases increase in dislocation density results in increase of corrosion resistance. Huang et al. [59] reported improvement in passivation behavior of Ti–25Nb–3Mo–3Zr–2Sn alloy post SMAT and attributed to high density of dislocations. Once a passive layer is formed, it acts as a barrier and results in improvement of corrosion resistance. The stability of the passive film is dependent on the interfacial bonding between the substrate and the film. The poor polarization resistance of the sandblast-annealed Ti was due to poor interfacial bonding between the passive film and the substrate resulting from high density of dislocation near the surface region [60]. Hence, it may be the increase in dislocation density which resulted in deterioration of corrosion resistance of the samples USSP treated for longer duration.

Significant improvement in corrosion resistance for the USSP 15 sample is thus due to ultrafine grain size and reduction in size of the second phase precipitates in combination with high dislocation density and lower surface roughness. These parameters in combination led to formation of adherent passive layer which ultimately enhanced the corrosion resistance of the 7075 aluminium alloy.

5. Conclusions

Grain refinement in the surface region was confirmed by X-ray diffraction and TEM analysis of the USSP treated specimens. SKPFM studies also confirmed the refinement of the second phase precipitates.

Potentiodynamic polarization showed improved ability for passivation with a decrease in corrosion current density after the USSP treatment. Electrochemical impedance spectroscopy revealed that polarization resistance R_p increased significantly and double layer capacitance (C_{dl}) was found to be decreased after the USSP treatment indicating lower corrosion activity on the metal surface/solution interface, compared to that of the without USSP. After prolonged immersion of 360 h in 3.5 wt% NaCl, the USSP 15 sample exhibited superior corrosion resistance which confirms that this surface treatment is effective even for longer service period.

The SEM/EDS results confirmed that pitting was probably associated with the cathodic second phase precipitates. Based on schematic it was proposed that due to lower galvanic coupling between the matrix and precipitates the USSP treated sample exhibited lower pitting tendency and also benefited in passive layer formation. The passive layer mainly constituted $Al(OH)_3$ with Al_2O_3 which was confirmed by XPS analysis.

All the samples USSP treated for different durations showed enhanced corrosion resistance as compared to that of the without USSP but the sample USSP treated for 15 s showed the best corrosion resistance amongst the all even after prolonged immersion in aggressive environment.

Appendix A. Supplementary material

Supplementary data associated with this article can be found, in the online version, at https://doi.org/10.1016/j.ultras.2018.08.011.

References

[1] C. Panagopoulos, E. Georgiou, A. Gavras, Corrosion and wear of 6082 aluminum alloy, Tribol. Int. (2009) (accessed June 6, 2017).
[2] M. Trueba, S. Trasatti, Study of Al alloy corrosion in neutral NaCl by the pitting scan technique, Mater. Chem. Phys. (2010) (accessed June 6, 2017).
[3] R. Ayer, J.Y. Koo, J.W. Steeds, B.K. Park, Microanalytical study of the heterogeneous phases in commercial Al-Zn-Mg-Cu alloys, Metall. Trans. A. 16 (1985) 1925–1936, https://doi.org/10.1007/BF02662393.
[4] M. Trueba, S. Trasatti, Study of Al alloy corrosion in neutral NaCl by the pitting scan technique, Mater. Chem. Phys. (2010) (accessed June 6, 2017).
[5] J. Park, A. Ardell, Precipitate microstructure of peak-aged 7075 Al, Scr. Metall. (1988) (accessed June 11, 2017).
[6] P. Premendra, H. Terryn, J. Mol, A comparative electrochemical study of commercial and model aluminium alloy (AA5050), Material (2009) (accessed June 11, 2017).
[7] C. Rhodes, M. Mahoney, W. Bingel, R. Spurling, Effects of friction stir welding on microstructure of 7075 aluminum, Scr. Mater. (1997) (accessed June 11, 2017).
[8] V. Pandey, G. Rao, K. Chattopadhyay, N.C.S. Srinivas, V. Singh, Effect of surface Nanostructuring on LCF behavior of aluminum alloy 2014, Mater. Sci. (2015) (accessed June 11, 2017).
[9] S. Kumar, K. Chattopadhyay, G. Mahobia, V. Singh, Hot corrosion behaviour of Ti–6Al–4V modified by ultrasonic shot peening, Mater. Des. (2016) (accessed June 11, 2017).
[10] B. Mordyuk, G. Prokopenko, M. Vasylyev, Effect of structure evolution induced by ultrasonic peening on the corrosion behavior of AISI-321 stainless steel, Mater. Sci. (2007) (accessed June 11, 2017).
[11] T. Wang, J. Yu, B. Dong, Surface nanocrystallization induced by shot peening and its effect on corrosion resistance of 1Cr18Ni9Ti stainless steel, Surf. Coatings Technol. (2006) (accessed June 11, 2017).
[12] X. Wu, N. Tao, Y. Hong, B. Xu, J. Lu, K. Lu, Microstructure and evolution of mechanically-induced ultrafine grain in surface layer of AL-alloy subjected to USSP, Acta Mater. 50 (2002) 2075–2084, https://doi.org/10.1016/S1359-6454(02)00051-4.
[13] L. Wen, Y. Wang, Y. Zhou, L. Guo, J.-H. Ouyang, Microstructure and corrosion resistance of modified 2024 Al alloy using surface mechanical attrition treatment combined with microarc oxidation process, Corros. Sci. 53 (2011) 473–480, https://doi.org/10.1016/j.corsci.2010.09.061.
[14] M. Laleh, F. Kargar, Effect of surface nanocrystallization on the microstructural and corrosion characteristics of AZ91D magnesium alloy, J. Alloys Compd. (2011) (accessed June 11, 2017).
[15] M. Kheradmandfard, S. Kashani-Bozorg, ... C. K.-U., undefined 2017, Nanostructured β-type titanium alloy fabricated by ultrasonic nanocrystal surface modification, Elsevier. (n.d.). http://www.sciencedirect.com/science/article/pii/S1350417717302559 (accessed January 23, 2018).
[16] S.V. Kumar Sanjeev, K. Chattopadhyay, S.R. Singh, Surface nanostructuring of Ti-6Al-4V alloy through ultrasonic shot peening, J. Surf. (2017) (accessed June 11, 2017).
[17] T. Wu, J. Wu, Effect of sulfate ions on corrosion inhibition of AA 7075 aluminum alloy in sodium chloride solutions, Corrosion (1995) (accessed June 11, 2017).
[18] K. Ralston, N. Birbilis, Effect of grain size on corrosion: a review, Corrosion (2010) (accessed June 11, 2017).
[19] S. Dan, J. Jiang, P. Lin, D. Yang, Corrosion behavior of ultra-fine grained industrial pure Al fabricated by ECAP, Nonferrous Met. Soc. China (2009) (accessed June 6, 2017).
[20] B. Chen, Surface nanocrystallization induced by shot peening and its effect on corrosion resistance of 6061 aluminum alloy, J. Mater. Res. 29 (2014).
[21] H. Krawiec, V. Vignal, H. Amar, P. Peyre, Local electrochemical impedance spectroscopy study of the influence of ageing in air and laser shock processing on the micro-electrochemical behaviour of, Electrochim. Acta (2011) (accessed June 6, 2017).
[22] M. Abdulstaar, M. Mhaede, L. Wagner, M. Wollmann, Corrosion behaviour of Al 1050 severely deformed by rotary swaging, Mater. Des. (2014) (accessed June 6, 2017).
[23] A. Kumar Singh, S. Ghosh, S. Mula, Simultaneous improvement of strength ductility and corrosion resistance of Al2024 alloy processed by cryoforging followed by ageing, Mater. Sci. Eng. A. 651 (2016) 774–785, https://doi.org/10.1016/j.msea.2015.11.032.
[24] B.D. Cullity, Elements of X-ray diffraction, 1978. http://www.sidalc.net/cgi-bin/

wxis.exe/?IsisScript=UCC.xis&method=post&formato=2&cantidad=1&expresion=mfn=042544 (accessed June 28, 2018).
[25] G. Williamson, W.H. Hall, X-ray line broadening from filed aluminum and wolfram, Acta Metall. 1 (1953) 22–31 (accessed June 28, 2018).
[26] J. De Wit, Local potential measurements with the SKPFM on aluminium alloys, Electrochim. Acta (2004) (accessed June 11, 2017).
[27] O.S. Fet Heakal, NS Tantawy, Influence of chloride ion concentration on the corrosion behavior of Al-bearing TRIP steels, Mater. Chem. Phys. 130 (2011) 743–749.
[28] U. Trdan, J. Grum, Evaluation of corrosion resistance of AA6082-T651 aluminium alloy after laser shock peening by means of cyclic polarisation and ElS methods, Corros. Sci. (2012) (accessed June 11, 2017).
[29] M. Dominguez-Crespo, A. Torres-Huerta, XPS and EIS studies of sputtered Al–Ce films formed on AA6061 aluminum alloy in 3.5% NaCl solution (accessed June 6, 2017), J. Appl. (2010) (accessed June 6, 2017).
[30] H. Lee, D. Kim, J. Jung, Y. Pyoun, K. Shin, Influence of peening on the corrosion properties of AISI 304 stainless steel, Corros. Sci. (2009) (accessed April 12, 2016).
[31] K. Krishna, K. Sivaprasad, T. Narayanan, Localized corrosion of an ultrafine grained Al–4Zn–2Mg alloy produced by cryorolling, Corrosion (2012) (accessed June 8, 2017).
[32] Surface modification of laser-and shot-peened 6082 aluminium alloy: laser peening effect to pitting corrosion, Int. J., 2011. http://www.emeraldinsight.com/doi/abs/10.1108/17579861111108572 (accessed June 8, 2017).
[33] F. Song, X. Zhang, S. Liu, Q. Tan, D. Li, The effect of quench rate and overageing temper on the corrosion behaviour of AA7050, Corros. Sci. (2014) (accessed June 8, 2017).
[34] D. Lopez, S. Simison, S. De Sanchez, Inhibitors performance in CO 2 corrosion: EIS studies on the interaction between their molecular structure and steel microstructure, Corros Sci (2005) (accessed June 11, 2017).
[35] B.M. Bilkova K, Hackerman N, No Title, Proc. NACE Corros. Pap. No. 2284, Denver, CO. (2002).
[36] J. Bessone, D. Salinas, C. Mayer, M. Ebert, An EIS study of aluminium barrier-type oxide films formed in different media, Electrochimica (1992) (accessed June 11, 2017).
[37] B. Dougherty, S. Smedley, J. Scully, D. Silverman, Electrochemical impedance: analysis and interpretation, ASTM STP (1993) (accessed June 11, 2017).
[38] K. Hladky, L. Callow, J. Dawson, Corrosion rates from impedance measurements: an introduction, Br. Corros. J. (1980) (accessed June 11, 2017).
[39] T. Hong, Y. Sun, W. Jepson, Study on corrosion inhibitor in large pipelines under multiphase flow using EIS, Corros. Sci. (2002) (accessed June 11, 2017).
[40] S. Das, I.B. Singh, M. Singh, A comparative corrosion behavior of Mg, AZ31 and... - Google Scholar, J. Magnes. Alloy 3 (2015) 142–148 (accessed November 28, 2017).
[41] F. Latief, E. Sherif, A. Almajid, H. Junaedi, Fabrication of exfoliated graphite nanoplatelets-reinforced aluminum composites and evaluating their mechanical properties and corrosion behavior, J. Anal. (2011) (accessed June 11, 2017).
[42] I. Singh, D. Mandal, M. Singh, S. Das, Influence of SiC particles addition on the corrosion behavior of 2014 Al–Cu alloy in 3.5% NaCl solution, Corros. Sci. (2009) (accessed June 11, 2017).
[43] K. Ghosh, S. Mukhopadhyay, B. Konar, Study of aging and electrochemical behaviour of Al Li Cu Mg alloys, Material (2013) (accessed June 11, 2017).
[44] G. Elewady, I. El-Said, A. Fouda, Anion surfactants as corrosion inhibitors for aluminum dissolution in HCl solutions, Int. J. Electrochem. Sci. (2008) (accessed June 11, 2017).
[45] F. Wall, M. Martinez, J. Vandenavyle, Relationship between induction time for pitting and pitting potential for high-purity aluminum, J. Electrochem. (2004) (accessed June 11, 2017).
[46] E. Sherif, Corrosion and corrosion inhibition of aluminum in Arabian Gulf seawater and sodium chloride solutions by 3-amino-5-mercapto-1, 2, 4-triazole, Int. J. Electrochem. Sci. (2011) (accessed June 11, 2017).
[47] H.J.E.S.M. Sherif, A.A. Almajid, F.H. Latif, Effects of graphite on the corrosion behavior of aluminum-graphite composite in sodium chloride solutions, J. Electrochem. Sci. (2011) (accessed June 11, 2017).
[48] J. Pang, F. Liu, J. Liu, M. Tan, D. Blackwood, Friction stir processing of aluminium alloy AA7075: Microstructure, surface chemistry and corrosion resistance, Corros. Sci. (2016) (accessed June 11, 2017).
[49] R. Inturi, Z. Szklarska-Smialowska, Localized corrosion of nanocrystalline 304 type stainless steel films, Corrosion (1992) (accessed June 11, 2017).
[50] V.O. Abramov, O.V. Abramov, F. Sommer, O.M. Gradov, 1998, Surface hardening of metals by ultrasonically accelerated small metal balls, Elsevier. (n.d.). https://www.sciencedirect.com/science/article/pii/S0041624X98000274 (accessed February 15, 2018).
[51] R. Revie, H. Uhlig, Uhlig's corrosion handbook, 2011. https://books.google.co.in/books?hl=en&lr=&id=UnYlthV6fxoC&oi=fnd&pg=PR17&dq=corrosion+handbook+(Wiley,+2011)&ots=MnLjyX2fkD&sig=QVgQ3GM6D2tvoEhixO-3UuUc1KA (accessed June 11, 2017).
[52] S. Dan, J. Jiang, P. Lin, D. Yang, Corrosion behavior of ultra-fine grained industrial pure Al fabricated by ECAP, Nonferrous Met. Soc. China (2009) (accessed June 11, 2017).
[53] S.O. In-Joon, H. Nakano, O.U. Satoshi, S. Kobayashi, H. Fukushima, Z. Horita, Trans. Nonferr. Met. Soc. Chn. 19 (2009) 904–908.
[54] R. Gupta, R. Raman, C. Koch, Fabrication and oxidation resistance of nanocrystalline Fe10Cr alloy, J. Mater Sci (2010) (accessed June 11, 2017).
[55] O. Takakuwa, H. Soyama, Effect of residual stress on the corrosion behavior of austenitic stainless steel, Adv. Chem. Eng. (2014) (accessed June 11, 2017).
[56] U. Trdan, J. Grum, SEM/EDS characterization of laser shock peening effect on localized corrosion of Al alloy in a near natural chloride environment, Corros Sci (2014) (accessed June 11, 2017).
[57] W. Li, D. Li, Variations of work function and corrosion behaviors of deformed copper surfaces, Appl. Surf. Sci. (2005) (accessed June 11, 2017).
[58] T. Balusamy, S. Kumar, T. Narayanan, Effect of surface nanocrystallization on the corrosion behaviour of AISI 409 stainless steel, Corros. Sci. (2010) (accessed June 11, 2017).
[59] R. Huang, Y. Han, The effect of SMAT-induced grain refinement and dislocations on the corrosion behavior of Ti–25Nb–3Mo–3Zr–2Sn alloy, Mater. Sci. Eng. C. (2013) (accessed June 11, 2017).
[60] X. Jiang, X. Wang, J. Li, D. Li, C. Man, Enhancement of fatigue and corrosion properties of pure Ti by sandblasting, Mater. Sci. (2006) (accessed June 11, 2017).